

Transparent Conductive Oxides and Their Applications in Near Infrared Plasmonics

Zhewei Wang, Chaonan Chen, Ke Wu, Haining Chong, and Hui Ye*

Transparent conductive oxides (TCOs) have been widely used as an important component of optoelectronic devices. They are required to exhibit high performance in both visible-range transparency and electronic conductivity simultaneously. In near infrared (NIR) wavelength, these highly doped semiconductor oxide materials exhibit a drop in their real part of dielectric permittivity from positive to negative. In other words, the epsilon-near-zero (ENZ) frequency of TCO is located in NIR spectral regime. On the other hand, the imaginary part of the permittivity is relatively low which implies less optical loss when compared to noble metals. This “metal-like” permittivity dispersion characteristic of TCOs means their capability to support surface plasmons (SPs) in the NIR regime. In this paper, a summary of various physical parameters of commonly used TCOs such as ITO, AZO, and FTO, etc., is given. These parameters include carrier density, carrier mobility, plasma frequency, and ENZ wavelength. The difference among these parameters determines their diverse performance in infrared range. In this paper, the important role of TCOs for applications in the NIR/IR wavelength ranges are reinforced, as they are demonstrated in the visible range.

1. Introduction

Transparent conduction oxides (TCOs), a unique branch of wide bandgap semiconductors, are traditionally recognized for their concurrent high conductivity and high transparency in visible range,^[1] which enable their widespread usage in photoelectronics. In recent years, the applications have further extended from low-e glass,^[2] transparent electrodes,^[3] and photovoltaics components^[4] to critical constituent materials in flexible display,^[5] meta-structures, as well as in transformation optics (TO).^[6] In particular, the permittivity (ϵ) dispersion behavior of most TCOs shows that the real parts of permittivity will reach zero in near-infrared range. Within these so-called epsilon-near-zero (ENZ) regions some interesting physical phenomena would occur, such as “superluminal speed”^[7] and


large nonlinearity.^[8] In the wavelengths longer than ENZ point, surface plasmon (SP) modes may be excited in the interface once the permittivity matching is met, which makes it possible to design and fabricate sub-wavelength ultra-compact NIR devices with TCOs to replace the noble metals.^[9–11]

Normally, TCOs are doped semiconductors including predominantly metal-oxides as SnO_2 , In_2O_3 , ZnO , and CdO , as well as doping elementals such as F, In, Ga, Al, Ti, and Cu, etc.^[12] Among all TCOs, AZO (Al: ZnO), ITO (Sn: In_2O_3), and GZO (Ga: ZnO) are the most common n-type candidates.^[6] However, so far, p-type TCOs, such as CuAlO_2 ,^[13] SrCu_2O_2 ,^[14] NiO_x ,^[15] have not been widely used as n-type TCOs, mainly due to their low carrier density.^[16] For instance, the carrier density of NiO films can only reach 10^{18} cm^{-3} ^[15] while the value of ITO is 10^{21} cm^{-3} .^[17] In recent years, it has been found that the carrier properties of materials are closely related to their

surface plasmons performance. Surface plasmons are defined as collective oscillations of free conduction electrons at the interface between two materials of opposite permittivity signs (negative and positive), whereby the resonance frequency of SPs corresponds to the material's charge carrier density. The carrier densities of noble metals, such as silver and gold are in the order of 10^{22} cm^{-3} ,^[18] helping them excite SPs in the visible range.^[19] With carrier densities one order lower than noble metals, TCOs made a splash in NIR SPs.^[6,19]

Noble metals are widely used as surface plasmon materials because of their advantages including long propagation length of SP mode, low penetrating depth into metals, large near-field enhancement, and wide applicable wavelength range (from visible to mid-infrared region).^[9] But in NIR range, TCOs could outperform metals with some virtues: The manufacturing process of TCOs is compatible with CMOS technology, high quality TCOs thin films can be readily fabricated by processes of chemical vapor deposition (CVD),^[20] physical vapor deposition (PVD),^[20,21] magnetron sputtering,^[22] etc. The optical losses of TCOs are less than metals and their optical properties are can be tuned over a wide range by adjusting the composition. In the NIR range, the imaginary part of gold's permittivity is very large, for instance, 10.97 at 1550 nm, while the imaginary part of ITO at 1550 nm is just around 0.6. A large imaginary part of permittivity means large optical loss, that may obstruct the applications. Noble metals, with elemental composition, are incapable of

State Key Laboratory of Modern Optical Instrumentation
College of Optical Science and Engineering
Zhejiang University
Hangzhou 310027, P. R. China
E-mail: huiye@zju.edu.cn

 The ORCID identification number(s) for the author(s) of this article can be found under <https://doi.org/10.1002/pssa.201700794>.

DOI: 10.1002/pssa.201700794

tuning their plasma frequency by composition alone. On the contrary, as most TCOs are non-stoichiometric or miscible, their electrical and optical parameters can be manipulated by fabrication conditions and doping concentration,^[23] which make them compact and easy to integrate.

It is rather noteworthy that enhanced optical nonlinearity has been reported recently in the near infrared range, especially at the epsilon-near-zero (ENZ) wavelength range of some TCO films.^[7,24] Simply considering the ideal lossless dielectric whose refractive index $n = \sqrt{\epsilon\mu}$ in optical range (where ϵ is permittivity and μ is permeability, for the common nonmagnetic materials, $\mu \approx 1$), we can get $n = \sqrt{\epsilon}$. Differential the above formula, the change in refractive index will be therefore written as $dn = d\epsilon/2\sqrt{\epsilon}$, as ϵ is in the dominator, that indicates when ϵ is near zero, a small change of permittivity will lead to a strong refractive index oscillation.^[25] Traditional electro-optic crystals have a small electro-optic coefficient, for example, the electro-optic coefficient γ_{33} of lithium niobate (LiNbO₃) is around 30 pm V⁻¹,^[26] which leads to a high half-wave voltage. The all-optical modulators also face the problem of low nonlinear coefficient. In ENZ range, TCOs provide a higher nonlinear coefficient, paving the way for the applications of all-optic modulators.

This paper intends to provide a review of fundamental principles, recent developments and applications of TCOs in near-infrared plasmonics. In Section 2, we provide a brief introduction of theory background. In Section 2.1, Drude and Lorentz model will be expressed to illustrate the trend that permittivity varies as a function of wavelength. With the increasing of wavelength, the real part of TCO's permittivity could reach near-zero range, that is what discussed in Section 2.2. surface plasmon occurs at longer wavelengths, where the real part of permittivity is negative. In Section 2.3, we raise the plasmonic resonance conditions and figure-of-merit to characterize them. In Section 3, we initially start talking about the general properties of TCOs including loss mechanism, then introduce unique characteristics and applications of them separately. The last section presents our perspective on future developments of TCOs on plasmonics.

2. Theory

2.1. Dispersion Model

Permittivity (ϵ) is an important inherent parameter of materials, and it is wavelength dispersive. As a complex type physical parameter, its real part is written as ϵ_r , which can change from positive to negative in some wavelength range for conductors and heavily doped semiconductors. The wavelength where ϵ_r cross zero is called as epsilon-near-zero (ENZ) point. The imaginary part of ϵ is written as ϵ_i , also shows dispersion behavior. Generally speaking, ϵ_r and ϵ_i are closely related to carrier density, carrier mobility, carrier effective mass and optical loss of materials.

Among the dispersion models which describe the permittivity dispersion properties, Drude model is for those which have a large number of free carriers such as metals, while Lorentz model performs better for bounded electrons in semiconductors.



Zhewei Wang received his bachelor's degree in optical engineering from Zhejiang University in 2014. He is currently a Ph.D student at Zhejiang University in the college of optical science and engineering. His current research interests include searching for improved plasmonic materials and integrated optoelectronic devices.



Hui Ye is a professor at college of optical science and engineering, Zhejiang University, China. He obtained the B.S. degree in department of material science and engineering, Zhejiang University in 1990, and the Ph.D degree in Shanghai institute of optics and fine mechanics, Chinese Academy of Science in 1995. He was once a visiting scholar in department of material science and engineering at University of California, Los Angeles (UCLA) and was a research scientist in department of applied physics at Hong Kong Polytechnic University, respectively. His research interests are focused on silicon photonics and surface plasma materials.

In the visible range, TCOs can be regarded as wide bandgap semiconductors, and Lorentz model is suitable to adequately describe their permittivity properties. According to Lorentz model,^[27,28] the permittivity is written as

$$\epsilon(\omega) = \epsilon_{\infty} + \frac{e^2}{\epsilon_0 m} \sum_n n \frac{N_{eh,n}}{(\omega_n^2 - \omega^2) - i\gamma\omega} \quad (1)$$

where ϵ_{∞} is the background permittivity and γ refers to the damping rates of free electrons which is given by $\gamma = \frac{1}{\tau}$. Here, τ is known as the relaxation time of the free electron gas and one can regard τ as the time taken for an electron to collide twice. ω_n is the resonance frequency, corresponding to electron transition energy.

As most TCOs are wide bandgap semiconductors,^[12] whose interband absorption is insignificant in infrared because of the insufficient energy of incident photons. TCOs' high carrier density makes them "metal like" in the infrared range. As a result, it is more precise to describe them with the Drude model,^[28] in which permittivity is written as:

$$\epsilon = \epsilon_{\infty} - \frac{\omega_p^2}{\omega^2 + i\gamma\omega} \quad (2)$$

where ϵ_{∞} and γ have the same meanings as those in the Lorentz model. The plasma frequency ω_p is characterized by $\omega_p = \sqrt{\frac{Ne^2}{\epsilon_0 m^*}}$ where N refers to carrier density, m^* is the effective mass of carriers in a semiconductor, e is electron charge, and ϵ_0 is

vacuum permittivity. Noble metals, such as silver and gold, have relatively high carrier densities exceeding 10^{22} cm^{-3} , locating their plasma frequencies in a range starts from the ultraviolet (UV) region to the visible light. TCOs have a lower conductivity and their carrier density can reach $10^{20} - 10^{21} \text{ cm}^{-3}$, an order lower than metals, shifting their plasma frequency to near-infrared range.

2.2. Epsilon Near Zero (ENZ) Regime

In normal dispersion, the real part of permittivity (ϵ_r) of material decreases as wavelength increases. When ϵ_r decreased from positive to negative, the wavelength is called as epsilon-near-zero (ENZ) wavelength. The ENZ wavelength of TCOs, depending on carrier density and preparation process, is always located in the near-infrared (NIR) range which is convenient for optical communication applications. For example, the ENZ wavelength of a 900 nm thick AZO thin film deposited by PLD is 1410 nm,^[8] while for a kind of commercial ITO is 1528 nm.^[25]

In the ENZ regime, a strong nonlinear optical coefficient has been revealed in AZO thin films.^[8] Suppose n_2 as the nonlinear refractive index then, the total refractive index can be written as $n = n_0 + \delta n_r$, where $\delta n_r = n_2 I$. In the ENZ regime, if ϵ_i is small enough and consequently the linear refractive n_0 would be tiny, thus the nonlinear refractive could make a significant effect. **Figure 1a** shows more than a 0.4 variation of AZO film refractive index using pump-probe measurement system, which is considered as a high change compared to the linear index of 0.09, around 500% of relative changes.^[8] Another similar experiment by Z-scan measurement has shown a 170% change of the linear refractive index in ITO.^[25] Nonlinearity results convey that TCOs have a promising future in optical nonlinear applications.

There are a few zero-index phenomena in TCOs. The phase velocity $v_{ph} = \frac{c}{\sqrt{\epsilon\mu}}$ can exceed c when $\epsilon \approx 0$ in ENZ regime ($\mu = 1$), where c is the speed of light in vacuum, ϵ and μ are permittivity and permeability, respectively. For instance, the light with a wavelength range from 1.11 to 1.25 μm exhibits superluminal in ITO.^[24] But a large frequency dispersion exists, there leads to a sub- c group velocity, where $v_g = \frac{\partial\omega}{\partial k}$, indicating

that the speed of energy and information is also lower than light in TCOs.

If imaginary part of permittivity (ϵ_i) approaches zero, the model of permittivity $|\epsilon| \approx 0$ may occur. According to non-resource Maxwell equation^[29]

$$\nabla \times \vec{H} = i\omega\epsilon\vec{E} \quad (3)$$

the interrelationship between electric and magnetic fields will no longer exist with an ϵ near zero. A gentle spatial variation of the magnetic field (left part of Equation 3) corresponds to a dramatic temporal variation of the electric field (a large ω in the right part of Equation 3), thereby space-time decoupling would occur,^[30,31] which produces a quasi-static electromagnetic wave. Hence, an electromagnetic wave can be guided through ENZ channel no matter how the channel is bent or distorted. It is explained that there is no phase change in the ENZ medium, and the length from the start to end of the channel can be seen as a point, just as **Figure 1b** shows.^[7] TCOs' optical losses (corresponding to the imaginary part of permittivity) are considerably low in their respective ENZ range. For example, the ϵ_i of AZO at ENZ regime is around 0.2, making it a promising future for these "near zero" applications.

2.3. Surface Plasmon (SP)

Surface plasmon (SP) is a kind of Transverse Magnetic (TM) wave which is usually occurring at the interface between metal and dielectric, enabling the material to focus the optical field in a narrow area around the interface.^[32,33] By solving Maxwell equation, we are able to obtain the plasmon wave-vector as $k_{SP} = k_0 \sqrt{\frac{\epsilon_m \epsilon_d}{\epsilon_m + \epsilon_d}}$, where ϵ_m and ϵ_d represent for the permittivity of metals and dielectric, respectively, k_0 is vacuum wavevector of incident light, k_{SP} is SP wave-vector.^[34] As k_{SP} is not equal to that of incident light in the same dielectric, a prism or grating coupling is necessary for exciting SP. Once the resonance condition is satisfied, namely, $\epsilon_m + \epsilon_d = 0$, the denominator will approach 0, that means SP resonance will be excited. Due to the ability to overcome diffraction limit, surface plasmon has the potential to be the basis of ultra-compact photonic devices. These

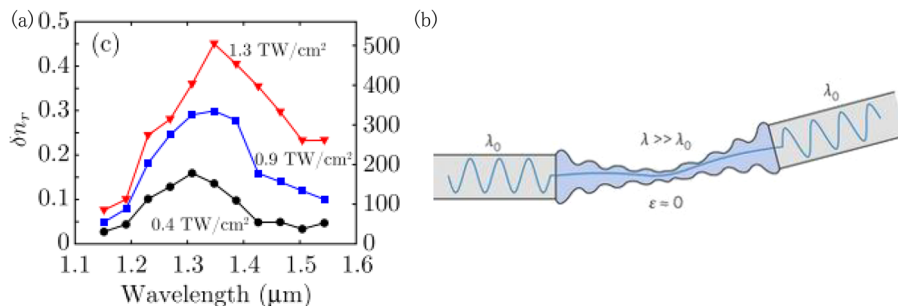


Figure 1. Nonlinear and zero-index phenomena in ENZ regime. a) The change of real part of refractive index ($\delta n_r = n_2 I$) versus wavelength. In around 1390 nm, the nonlinear refractive index change reaches maximum. Reproduced with permission.^[8] Copyright 2016, American Physical Society. b) A schematic view of tunneling effect of ENZ waveguide, where the phase of electromagnetic wave remains unchanged and exhibits "quasi-static". Reproduced with permission.^[7] Copyright 2017, Nature Research.

“metallic” materials can guide light like fibers with a much smaller size.^[11]

The surface plasmon confined in the area smaller than a cubic wavelength is called as localized surface plasmon (LSP),^[34] where optical field is localized in the vicinity of some microstructures (hot spots) without propagation. As for a spherical nanoparticle whose size is smaller than incident wavelength, the polarization adjacent to it is expressed as^[35]

$$\vec{P} = 4\pi a^3 \frac{\epsilon_m - \epsilon_d}{\epsilon_m + 2\epsilon_d} \quad (4)$$

where a is the radius of the sphere. When denominator becomes 0, namely, $\epsilon_m = -2\epsilon_d$, polarization increases dramatically, forming the effect of localized surface plasmon resonance (LSPR), where a significant enhancement of electric field at hot spots will be generated. The LSPR wavelength depends not only on the material type, but also on the shape and size of nanoparticles. For example, the resonant wavelength of gold nanorods can be tuned over a wide range by changing section area and lengths. One of its interesting and practical application is photothermal therapy.^[33] Gold nanoparticles are designed with large absorption cross-section but small scattering, which are fruitful for converting incident photons into thermal energy. With the help of concentrated heat, the nanoparticles are expected to play important roles to destroy cancer cells.^[36]

Figure of Merit (FOM) for a propagating surface plasmon (Q_{SPR}) and localized surface plasmon (Q_{LSP}) have been proposed to evaluate different kinds of surface plasmon materials.^[34] The respective FOM is defined as the ratio of enhanced electric field intensity to the incident one. For a propagating surface plasmon,^[37,38]

$$Q_{SPR} = \frac{\epsilon_r(\omega) + \epsilon_d(\omega)}{\epsilon_r(\omega)\epsilon_d(\omega)} \frac{[\epsilon_r(\omega)]^2}{\epsilon_i(\omega)} \quad (5)$$

where $\epsilon_r(\omega)$ and $\epsilon_i(\omega)$ stand for real and imaginary part of a metal permittivity, $\epsilon_d(\omega)$ represents permittivity of surrounding dielectrics, whose an imaginary part approaches to zero in the infrared operating region.

As for LSPR, whose FOM corresponds with the shapes of microstructures, we then choose sphere as a representative,^[37,38]

$$Q_{LSPR} = \frac{-\epsilon_r(\omega)}{\epsilon_i(\omega)} \quad (6)$$

A comparison of figure-of-merit for different TCOs and noble metals is provided in **Table 1**. Large Q factors represent strong ability for local field enhancement. Conventional metals, such as gold and silver, still have large figure-of-merit in the infrared range, making them the first choice in surface plasmon.^[39,40] For example, at a wavelength of 1550 nm in the communication band, the Q factor of gold is three orders of magnitude larger than that of TCOs.^[37] But the real part of gold's permittivity is largely negative in the infrared range (e.g., -95.92 @ 1550 nm^[41]), making it hard to find an appropriate dielectric to meet resonance condition ($\epsilon_r + \epsilon_d \approx 0$ at resonant wavelength). The optical losses of noble metals are significant. For example, the imaginary part of gold is 10.97 at 1550 nm, while that of TCOs is no more than 0.60. In order

to make an exhaustive comparison, Table 1 lists plasma wavelength (λ_p), ENZ wavelength, resistivity (ρ), carrier densities (N), the imaginary part of permittivity (ϵ_i) at ENZ wavelength, as well as Q factors of various materials. Plasma wavelength is calculated by $\lambda_p = \frac{2\pi c}{\omega_p}$ where ω_p is the same in the Drude model (Equation 2), implying the absorption cross section of the free carrier.^[42] Plasma frequency is dovetailing with carrier density and effective mass of carriers. A kind of material with smaller plasma frequency usually implies larger carrier density or lower effective mass of carrier.

As shown in Table 1, the ENZ regime of TCOs locates in infrared region. TCOs can support surface plasmon modes in infrared while maintaining the low loss. Noble metals may have a limit in photonics because they aren't compatible with the CMOS process. At this time, easy-fabricated, easy-integrated, and low-loss tunable TCOs are coming into the stage.

3. Materials

Currently widely used TCOs include indium tin oxide (ITO), fluorine doped tin oxide (FTO), aluminum doped zinc oxide, and gallium doped zinc oxide (AZO/GZO). Recently researchers still discover new types of TCOs, such as doped cadmium oxide and doped titanium oxide. More properties of TCOs are illustrated in ENZ and surface plasmon applications. Moreover, graphene, spinel type oxides, and correlated metals also show a good transparency and conductivity in the visible and near-infrared ranges, which introduce them as worthy candidates.

Plasma frequency (ω_p) and optical loss (γ) are the main factors influencing the performance of TCOs in the IR range. In Equation 2, permittivity (ϵ) can be divided into real and imaginary parts as

$$\epsilon(\omega) = \epsilon_\infty - \frac{\omega_p^2}{\omega^2 + \gamma^2} + i \frac{\omega_p^2 \gamma}{\omega(\omega^2 + \gamma^2)} \quad (7)$$

where each symbol has the same meaning as that in section 2.1. When the real part of permittivity approaches to zero, namely at ENZ regime, frequency ω satisfies the requirement as $\epsilon_\infty = \frac{\omega_p^2}{\omega^2 + \gamma^2}$, which can be transformed into

$$\omega(\text{ENZ})^2 = \frac{\omega_p^2}{\epsilon_0} - \gamma \quad (8)$$

where plasma frequency is expressed as $\omega_p \propto \sqrt{\frac{N}{m^*}}$. That means higher carrier density results in blue-shift of ENZ regime, that is why surface plasmon can be supported at a shorter wavelength. As most TCOs have approximately the same effective mass of carriers (around $0.1\text{--}0.3m_0$),^[43] their plasma frequencies are therefore dependent on carrier density. The near-infrared ENZ frequency means a relatively large carrier density (above $10^{20}\text{--}10^{21}\text{ cm}^{-3}$). Generally, carrier density can be modified by the doping process. Meanwhile, defects and crystallinity of TCOs also play an important role in their carrier densities. Films with good crystallinity and low defects possess higher carrier density in the same doping level. Besides, there is an optimal value of the doped element due to the solubility limit. The optimal concentration of In:CdO is 10%,^[44] while it is 5% for Ti:CdO.^[45]

Damping rates (γ) of free electrons correlate to optical losses, including optical absorption and scattering. Since TCOs are

Table 1. Comparison of some TCOs, noble metals and graphene, including plasmonic wavelength (λ_p), wavelength at ENZ, resistivity (ρ), carrier density of materials, figure-of-merit (Q) for SPP and LSPR, as well as imaginary part of permittivity (ϵ_i) at ENZ.

Materials		Plasmonic wavelength λ_p [nm] ^{c)}	Wavelength at ENZ [nm]	Resistivity ρ [Ω cm]	Carrier Density N [cm^{-3}]	Imaginary part of permittivity (ϵ_i) at ENZ	Q_{SPP} at 1550 nm	Q_{SPP}	Q_{LSPR}
Noble metals	Ag ^[18,37,125]	135	243	1.55×10^{-6}	5.8×10^{22}	3.26	4530	23413 (1.08 μm)	392 (1.08 μm)
	Au ^[37,126]	140	207	2.2×10^{-6}	6.6×10^{22}	3.39	1140	1410 (1.94 μm)	16.66 (0.89 μm)
Transparent conductive oxides	ITO ^[75,77]	696	1528	2.41×10^{-4}	1.34×10^{21}	0.60	0.39	2.72 (2.3 μm)	16 (2.3 μm)
	AZO ^[37,75]	820	1410	4.7×10^{-4}	1.23×10^{21}	0.36	1.46	33.1 (2.5 μm)	3.28 (2.2 μm)
	GZO ^[6,75,127]	643	1420	$7.9 \times 10^{-4\text{c)}$	$6.82 \times 10^{20\text{c)}$	0.35	0.923	15.96 (2.5 μm)	1.8 (2.3 μm)
	FTO ^[109]	1058	2110	8.0×10^{-4}	9.97×10^{20}	1.39	NA	12.69 (6 μm)	1.02 (4 μm)
	In:CdO ^[45]	946	1442	1.17×10^{-4}	8.86×10^{20}	0.39	0.321	3.75 (1.7 μm)	3.98 (1.7 μm)
	Dy:CdO ^[94]	–	1860	$2.5 \times 10^{-4\text{c)}$	3.7×10^{20}	0.48	NA	459.24 (5 μm)	49.08 (2.96 μm)
	Sn:CdO ^{[93]b)}	–	–	2.38×10^{-5}	4.74×10^{20}	–	–	–	–
	Graphene ^{[18]b)}	1900	–	5×10^{-6}	$< 10^{13} \text{ cm}^{-2}$	–	–	–	–
Correlate metal	SrVO ₃ ^[43]	932	1377	$2.8 \times 10^{22\text{c)}$	2.26×10^{22}	1.22	45.26	52.08 (1640 μm)	(1466 μm)

Plasmonic frequency (ω_p) is reverted to wavelength in order to comparison with ENZ wavelength. Q takes the maximum value at the wavelength in parentheses. For convenience, a column with Q_{SPP} at 1550 nm was listed.

^{a)} The substrate of Sn:CdO is MgO <111>; ^{b)} Graphene is 2D material, the unit of carrier density of graphene is cm^{-2} instead of cm^{-3} ; ^{c)} Besides FOM, these data are not given directly by literature but calculated. $\lambda_p = \frac{2\pi c}{\omega_p}$, $N = \frac{\omega_p^2 \epsilon_0 m^2}{e^2}$, and $\rho = \frac{1}{Neq}$.

wide-gap semiconductors, the energy of infrared photons is unable to excite interband transitions. Therefore, the total absorption mainly originates from an intraband absorption, where free carrier absorption (FCA) plays an important role. The carrier density is directly proportional to FCA. As the conductivity of material is proportion to both carrier density and mobility, a method to decrease the FCA is to reduce carrier density of TCOs and increase their carrier mobility. However, if N is controlled below 10^{19} cm^{-3} , the ENZ point will redshift toward the mid-infrared region.

Meanwhile, the scattering caused by interfaces and defects is another source of optical loss. These losses are caused by fabrication process. Therefore, more fabrication methods are raised to increase the crystallinity and inhabit defects, in order to reduce optical loss of TCOs. The fine control of the film growth process helps to improve its properties.

3.1. Tin Doped Indium Oxide (ITO) and Indium Oxide based TCOs

3.1.1. ITO

With high transparency in visible range (>95%) and resistivity as low as $10^{-4} \Omega \text{ cm}$, Indium Tin Oxide (ITO) performs outstandingly as a TCO.^[46] It can be manufactured by various

methods including magnetron sputtering,^[47] pulsed laser deposition,^[48] and chemical vapor deposition,^[49] or even wet process.^[50] Even in high temperature and humid environments, ITO performance is very stable.^[51,52] For a long time, ITO is widely used as electrode material and necessary component in low-e glass, solar cells, flat display devices.^[53] ITO is a kind of non-stoichiometric mixture consists of 90% In₂O₃ and 10% SnO₂ in most commercial uses.^[54] The permittivity has been obtained from ellipsometry measurement with Drude model fitting.^[48] With carrier density as high as 10^{21} cm^{-3} , the ENZ wavelength of ITO locates around 1.5 μm communication band, and its electrical and optical properties can be tuned by various methods.^[55,56] For instance, in the magnetron sputtering process, the increment of oxygen ratio will increase transparency but decrease conductivity, while the annealing in nitrogen will reduce oxygen defects and significantly increase conductivity.^[57,58] In application, applying an electric field can change the dielectric constant distribution of ITO.

Since the fact that the small change of ϵ can induce a large change of n at the ENZ wavelength, the footprint of the ITO-based electro-optic modulator can be smaller than that of conventional modulators. In the ENZ band, the refractive index change of ITO induced by electro-optic effect is 3–4 orders of magnitude larger than that of lithium niobate.^[59] As shown in **Figure 2a**, the modulation depth of 5 dB in 1.55 μm ^[60] can be obtained by the ITO-based tunable directional coupler.

Figure 2b shows, ITO's permittivity can be tuned approaching zero by applying 2.3V voltage. At this time, the light would be localized in plasmon mode at the ITO-HfO₂ interface, resulting in attenuated output power (off state). Once the voltage is removed, the output power will return to its original state (on state).

ITO is also introduced in the applications such as metamaterials,^[61–64] ultrafast switch,^[61] and hyperbolic metamaterial^[65] that mainly due to its ultrafast response and low loss in infrared range. Although ITO performs excellently in TCOs, sometimes ITO can't meet the application needs. Consequently, more indium oxide based materials were developed.

3.1.2. Other Doped Indium Oxides

In some occasions when low losses are required, new doped indium oxide is considered. In recent ten years, Ti⁴⁺,^[66,67] W⁶⁺,^[68] Mo⁵⁺,^[69,70] Zr⁴⁺,^[71] H⁺,^[53,72] and Ce⁴⁺^[73] have been reported as dopants with high performance for Indium oxides, all of which are reported to have higher carrier mobility compared with Tin doped Indium oxide (ITO). Among them, Hydrogen doped Indium Oxide (IO:H) was fabricated in 2007 by magnetron sputtering with H₂O vapor as Hydrogen source.^[53] The oxygen deficiencies are eliminated, and carrier scattering inside amorphous or crystalline lattice would be reduced by hydrogen doping,^[72,74] thus promoting carrier mobility and indium oxide conductivity. The carrier density of IO:H reaches $4.6 \times 10^{20} \text{ cm}^{-3}$, enabling SPPs in NIR and MIR range. More improvement was introduced by cerium oxide. Besides its similar ionic radius, CeO₂ can inhabit oxygen vacancies when doping with a large standard enthalpy of formation. Cerium oxide affords to IO:H (1.3% doped hydrogen) carrier mobility of $141 \text{ cm}^2 \text{ V}^{-1} \text{ s}^{-1}$ ^[73] and the plasma wavelength locates at $2.58 \mu\text{m}$ that qualify it for many applications which will be in the exploring phase. With magnetron sputtering process, the carrier mobility of Zr⁴⁺, Mo⁵⁺, W⁶⁺, Ti⁴⁺ doped Indium oxides can reach 160,^[71] 93,^[69] 358,^[68] and $45 \text{ cm}^2 \text{ V}^{-1} \text{ s}^{-1}$,^[66] respectively.

3.1.3. ITO Composites

Because of the low solid-solubility limits of dopants and low ionization efficiencies, further improvement of TCO carrier concentration faces significant challenges.^[75] Although metal shows a larger loss, it offers the best confinement-propagation balance compared with TCO even in the NIR region.^[76] Accordingly, the niche application of TCOs as NIR plasmonic materials requires the introduction of noble metals, to improve their overall performance. Our previous work shows sandwich structures as ITO/Au/ITO^[77] (Figure 3a) and ITO/TiN/ITO^[22] (Figure 3b) will significantly improve ITO's conductivity. Table 2 lists the various ITO composites and related measurements we performed to tune the electronic properties of ITO. The carrier densities are increased by a factor 2–10 times. Resulting in shorter ENZ wavelength, promoting their FOM in NIR range. With post-annealing, a co-sputter ITO with a silver sample can get an adjustment for ENZ of 300 nm. A Kretschmann prism was used to couple the incident light into SPP mode at 1550 nm (Figure 3c). Comparing to pure ITO, the deeper dip of reflectance of ITO/TiN/ITO sandwich structure indicates a better SPP coupling ability.

3.2. Al Doped ZnO (AZO) and Ga Doped ZnO (GZO)

AZO and GZO are widely used TCOs in part because they are non-toxic and refractory. Moreover, AZO's infrared loss is relatively low among TCOs for plasmonic applications in communication band.^[78,79] Facing the shortage reserves of Indium, ZnO based TCOs draw people's attention because of their abundant reserves.^[80] In AZO or GZO, the substitution of Al³⁺ or Ga³⁺ for Zn²⁺ provides an excess of electrons, forming n-type semiconductors.^[81] By adjusting dopant concentration, one can get various distributions of refractive index and even gradient-index in AZO/ZnO or GZO/ZnO mixtures. Meanwhile, there are many well-developed methods that facilitate the manufacture of AZO or GZO, such as magnetron sputtering, chemical vapor deposition, pulsed laser deposition.^[82] The permittivity of GZO/AZO becomes negative (show "metal like"),

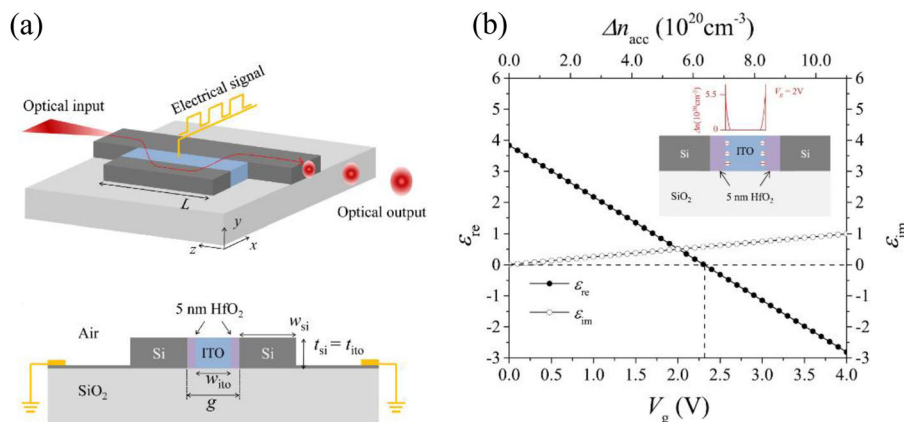


Figure 2. ITO based electro-optic modulator (a) schematic view of EO modulator. b) ϵ of ITO versus applied voltage at 1550 nm. ϵ_r reaches 0 at 2.3V applied. Reproduced with permission.^[60] Copyright 2016, IOP Publishing.

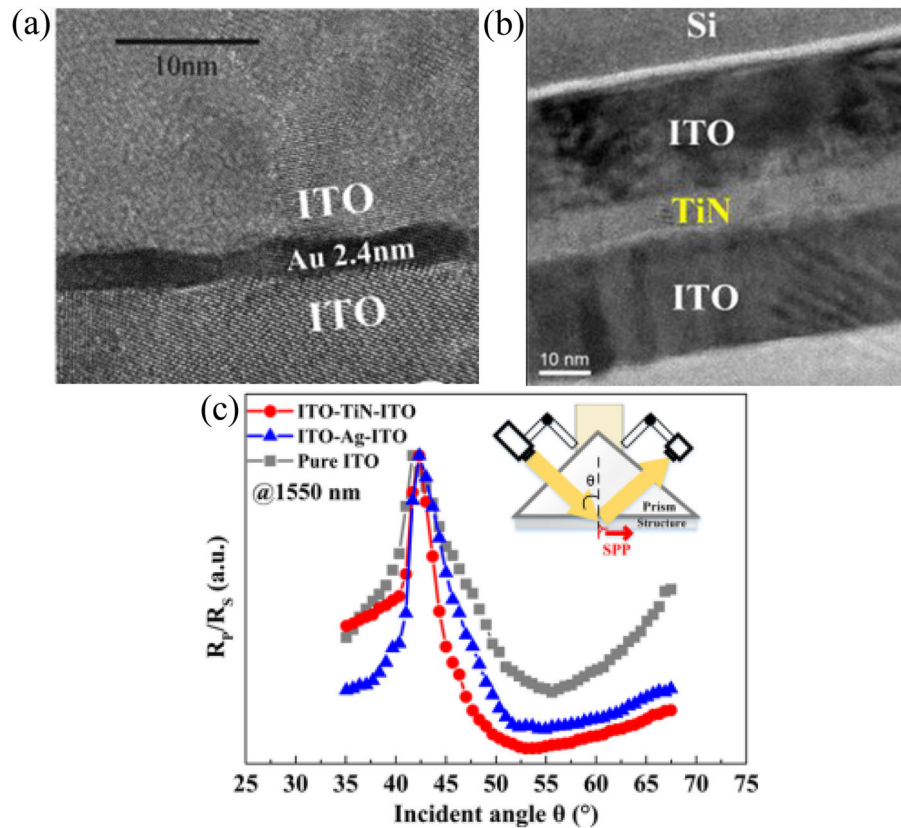


Figure 3. ITO-metal composite. TEM cross-section view of (a) ITO/Au(2.4 nm)/ITO sandwich structure and (b) ITO/TiN(9 nm)/ITO sandwich structure. a,b,) Reproduced with permission.^[22] Copyright 2018, American Chemical Society. c) Reflectance curves measured by Kretschmann prism coupling for ITO composite and pure ITO films. Only p-polarized reflectance light is able to couple into surface plasmonic (SP) mode. In around 50°, a reflectance dip is observed, indicating the SP mode is excited. c) Reproduced with permission.^[77] Copyright 2014, American Chemical Society.

while that of ZnO is still positive at the same infrared wavelength, acting as “dielectric”. As a result, it is easy to satisfy SP resonance condition $\epsilon_m + \epsilon_d = 0$, which makes them suitable for applications in metamaterials research field.^[83]

One kind of GZO/ZnO based polarization controlling metasurface^[84] acts as a quarterwaveplate (QWP), as shown in **Figure 4**. Thanks to LSPR originated from GZO, the reflections for orthogonal direction, x (along with the strip) and y (perpendicular to the strip) are different. As a result, the reflection of co-polarized and cross-polarized direction are different, too. Within the wavelength range where the ratio of

co- and cross-polarized reflection approached to one, the phase of reflected light was delayed about 45° compared to incident light. The operation bandwidth of such QWP is as long as 450 nm from $\lambda = 1.75 \mu\text{m}$ to $\lambda = 2.2 \mu\text{m}$.

Another application is LSPR enhanced absorption. As **Figure 5** shows, the structure consists of four-layer nanodisk array, where GZO with a carrier density of 10^{21} cm^{-3} acts as a metal and ZnO with a carrier density of 10^{16} cm^{-3} acts as a dielectric, in order to satisfy equation $\epsilon_m = -2\epsilon_d$ in resonance. LSPR happens in the vicinity of the nanodisks, causing a strong absorption (dip in transmitted spectrum). The diameter of single nanodisk is

Table 2. Comparison of ITO, ITO/metal/ITO sandwich and ITO composite.

Material	Carrier density [cm^{-3}]	Carrier mobility [$\text{cm}^2 \text{V}^{-1} \text{s}^{-1}$]	Wavelength of ENZ [nm]	Q_{SPP}
ITO ^[17]	1.34×10^{21}	36.4	1528	16 (2.3 μm)
ITO/TiN/ITO ^[22]	1.62×10^{22}	16	775	110 (2.0 μm)
ITO-Ag ^[47]	2.41×10^{21}	12	1510	20 (2.3 μm)
ITO-Ag (annealing) ^[47]	6.02×10^{21}	12	1170	12 (1.8 μm)
ITO/Au/ITO ^[77]	2.61×10^{21}	7.2	973	21 (2.0 μm)

Carrier density, carrier mobility, wavelength of ENZ, and figure-of-merit are listed. Q takes the maximum value at the wavelength in parentheses.

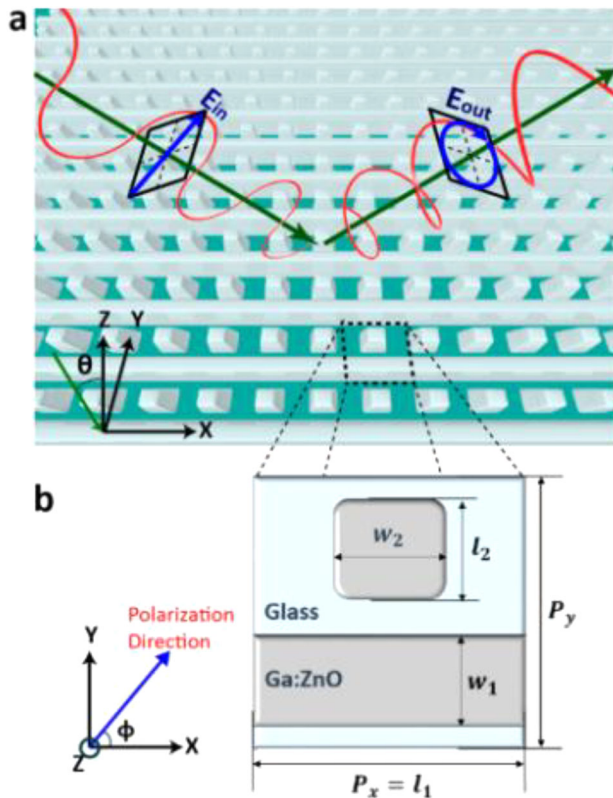


Figure 4. GZO/ZnO based polarization controlling metasurface: a) schematic of the metasurface. θ is the incident angle. b) A schematic view of unit cells of the metasurface, where ϕ is the polarization angle. Reproduced with permission.^[84] Copyright 2016, American Chemical Society.

several hundred nanometers, less than operating light's diffraction limit (over 1 micrometer), implying a good performance in light confinement application.^[85] Such nanodisk array configuration can also be used effectively as chip structure in surface enhanced infrared absorption spectroscopy (SEIRA) measurements. Covered by octadecanethiol (ODT) layer and measured by Fourier Transform Infrared spectroscopy (FTIR), the nanodisk array showed some deep dips of reflectivity in mid-

and near-infrared ranges, represents absorption from symmetric CH_2 stretch (2848 cm^{-1}), symmetric CH_3 (2871 cm^{-1}), antisymmetric CH_2 stretch (2915 cm^{-1}), antisymmetric CH_3 (2957 cm^{-1}), besides, the varying geometric dimensions of nanodisks could change resonant wavelength from 1.7 to $5\text{ }\mu\text{m}$.

3.3. Doped Cadmium Oxide

As the first TCO ever discovered, CdO was fabricated and studied in 1907.^[86] Because of its toxicity and low conductivity, CdO gave way to ITO, AZO.^[18] II–VI semiconductor CdO has a rock-salt structure, and it's easy to increase carrier density by introducing Group III element (B,^[87] Al,^[88] In,^[45] Ga,^[45] Sc,^[89] Y,^[90] Ti^[91]) or transition metal element (Ti,^[45] V,^[45] Fe,^[92] Sn,^[93] Dy^[94]) as donors. Group III element provides two outermost electrons in bonding, and the extra outermost electron as a carrier. While transition metal provides two 4s electrons in bonding, but their donor level is dependent on 3d electrons. This different electron configuration leads to doping-dependent mobility. The former has a higher carrier mobility than the latter. The carrier mobility of doped CdOs is higher than that of ITO ($36.4\text{ cm}^2\text{ V}^{-1}\text{ s}^{-1}$).^[17] The highest mobility of $609\text{ cm}^2\text{ V}^{-1}\text{ s}^{-1}$ was obtained in Sn:CdO grown on MgO substrate with $\langle 111 \rangle$ orientation. On top of that, Sn doped CdO has a good conductivity ($16\,000\text{ S cm}^{-1}$)^[93] at a low carrier density.

The carrier density of highly doped CdO could reach the order of 10^{20} cm^{-3} . The tunability of ENZ wavelength from 1600 to 1300 nm ^[87] makes it a potential candidate for SP material in telecommunication band. For example, Dy:CdO has a good performance in mid-IR with a Q_{SPP} as high as 459.24 at the wavelength of $5\text{ }\mu\text{m}$ (carrier density $3.70 \times 10^{20}\text{ cm}^{-3}$).^[94]

3.4. Doped Titanium Dioxide (TiO_2)

TiO_2 , a wide band semiconductor, is usually used for optical coating and photocatalytic. In spite of weak conductivity of pure TiO_2 , researchers have recently realized its potential as TCOs by doping technique.^[95,96] Group V elements, such Nb and Ta, are introduced to replace the sites of Ti, in order to reduce their resistivity.^[97] Anatase and rutile are two phase of titanium oxide

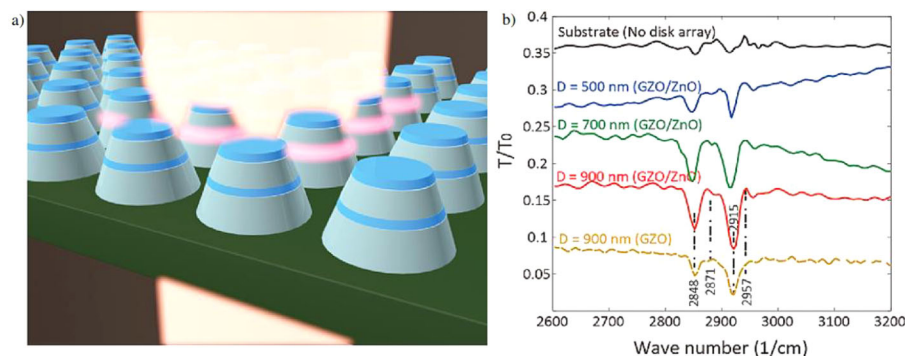


Figure 5. GZO/ZnO nanodisks arrays. a) Schematic of localized surface plasmon resonance enhanced absorption of GZO/ZnO nanodisks b) SEIRA absorption peak of octadecanethiol. Reproduced with permission.^[85] Copyright 2015, American Chemical Society.

crystal forms, where doped rutile TiO_2 shows resistive, but doped anatase TiO_2 is semiconductor.^[98] The conductivity of 5% Ta^[99] doped anatase TiO_2 (TTO) and 6% Nb doped anatase TiO_2 (NTO) are reported to be $2.5 \times 10^{-4} \Omega^{[100]}$ and $4.6 \times 10^{-4} \Omega^{[101]}$ respectively. This is caused by d-electrons, similar to transition metal doped CdO. It's easy to obtain large carrier densities of TTO and NTO^[102], for example, an NTO sample with carrier density of $1.3 \times 10^{21} \text{ cm}^{-3}$ ^[103] is prepared by magnetron sputtering. However, the carrier mobility of both NTO and TTO are restricted, for instance, a TTO sample fabricated by PLD possess mobility of $12.5 \text{ cm}^2 \text{ V}^{-1} \text{ s}^{-1}$ ^[100] is reported.

Besides, an abnormal dispersion is reported in infrared range in nitrogen annealed TiO_2 (TiO_xN_y). **Figure 6**^[104] shows that TiO_xN_y (N atoms replace the position of O atoms in annealing process) has two ENZ wavelength range (700–850 nm and 1100–1350 nm). The abnormal phenomenon can be attributed to the mixture of TiN and TiO_x phase in the film. With the increment of nitrogen pressure in annealing, the double ENZ region expands and then shrinks. When the content of TiN saturates, the double ENZ disappears. Furthermore, the two ENZ wavelengths can be tuned by varying nitrogen partial pressure in annealing, making it a potential material in plasmonic application.

3.5. Fluorine Doped TCOs

In addition to cationic doping, oxygen can be substituted by other anions. For example, fluorine doped tin oxide (FTO) has been widely used in low-emissivity windows since the 70th of the last century.^[105] Fluorine possesses many advantages in the doping of TCOs. Firstly, the radii of O^{2-} and F^- are similar, which could prevent lattice mismatch in doping; next, the introduction of fluorine would inhibit formation of oxygen vacancies;^[106] then, it's easy to prepare F doped TCOs by CVD, spray-pyrolysis, and other low-cost technology. Due to the fact that electrons are readily trapped in fluorine sites, fluorine doped TCOs show

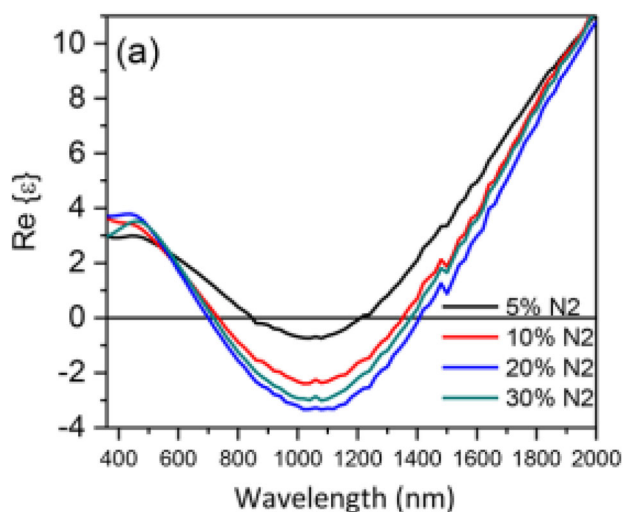


Figure 6. Abnormal dispersion of TiO_xN_y , inducing two ENZ region. One is 700–850 nm, the other is 1100–1350, respectively. Reproduced with permission.^[104] Copyright 2017, American Chemical Society.

limitations in electron mobility ($15.3 \text{ cm}^2 \text{ V}^{-1} \text{ s}^{-1}$ ^[107] comparing to $36.4 \text{ cm}^2 \text{ V}^{-1} \text{ s}^{-1}$ for ITO).^[52,108] Surface plasmon properties of fluorine doped tin oxides and their applications in mid-infrared are reported recently.^[109,110] With the aids of grating coupling, SPP modes are successfully excited by a 7.5 μm and a 10 μm periodic grating, respectively, showing two absorption bands located at 8 and 10.3 μm in FTIR spectrum, respectively.

More experiments of SPPs on fluorine doped Cadmium Oxide (FCO)^[106] are also reported. With the amount of doped F changing, the carrier density of FCO varies from $3.1 \times 10^{19} \text{ cm}^{-3}$ to $1.57 \times 10^{20} \text{ cm}^{-3}$, causing the SPP wavelength blue-shift from 5556 to 2726 nm.

3.6. Graphene

As a new-developing two-dimension (2D) material, graphene has drawn people's eyeballs because of ultra-fast carrier mobility and unique energy band structure. Every atomic monolayer of graphene has a permanent 2.3% absorbance^[111] of incident light in visible and NIR range, hence it is used in transparent electrodes. Graphene behaves as a metal rather than a semiconductor since the free electrons of graphene are permeated in an electron cloud (electrons in graphene are non-scattered^[52]), instead of being localized in the lattice.^[6,80] These "metal like" electrons are easy to support SPs. Graphene is widely used in applications of electro-optic modulator,^[59] optical switch, optical resonator,^[112] and metamaterials^[113] in mid-IR^[114] and THz range.

However, comparing to traditional semiconductors, graphene is difficult^[115,116] to fabricate as single layers. Furthermore, in spite of the carrier mobility of graphene exceeds $10\,000 \text{ cm}^2 \text{ V}^{-1} \text{ s}^{-1}$, its carrier density is lower than TCOs, restricting its application in NIR. Though doped graphene could improve the ability to support SPs,^[117] it would inevitably reduce the transparency. And the issue of how to balance graphene's fabrication, transparency and carrier density still need to be studied.

3.7. Correlated Metals

It's an attractive idea for metals to be a transparent conductor. An ultra-thin metal film is required to obtain good transparency.^[118] However, if metals' thickness is less than the electron mean free path (EMFP),^[119] the surface scattering would be enlarged, resulting in low conductivity. The EMFP of gold and silver are 50 nm and 52 nm,^[120] respectively, which are too thick to maintain high transparency. Recent proposed correlated metals, such as SrVO_3 and CaVO_3 , have a low EMFP less than 6 nm. The effective mass m^* can be expressed as $m^* = m_{\text{band}}^* / Z_k$, where Z_k represents renormalization factor and m_{band}^* stands for the effective mass of carriers calculated by band theory. Commonly, the electrons of metals have no interaction thus Z_k equals 1. In correlated metals, electrons interact strongly, which makes $Z_k < 1$, and hence reduce the effective mass. Taking SrVO_3 as an example, the carrier density reaches $2.6 \times 10^{22} \text{ cm}^{-3}$ and the ENZ wavelength is 1337 nm,^[43] making it as an excellent candidate for surface plasmon in near-infrared region. With

good transparency (>80%) and low resistivity ($10^{-5} \Omega \text{ cm}^{[43,121]}$), correlated metals have a promising future as plasmonic material in the infrared wavelength range.

3.8. Spinel type oxides nanocrystals

Spinel-type oxides have a general chemical formula $A_2B_4O_4$, in which A^{3+} cations occupy octahedral sites (O_h) and B^{2+} cations occupy tetrahedral sites (T_d). Antisite defects could be shown when B^{2+} cations occupy O_h sites or A^{3+} cations occupy T_d sites. If an A^{3+} cation moves from O_h site to T_d site with a remaining valence +3, a donor defect will be formed; on the contrary, if a B^{2+} cation moves from T_d site to O_h site, remaining its valence +2, an acceptor defect will be formed.^[50,122] Antisites defects are common because the orbit radii of A^{3+} and B^{2+} cations are similar. Besides, off-stoichiometry defects (the ratio of A:B:O isn't 2:1:4) can also be used to tuning the doping level of spinel-type oxides.^[123] A GFO (Ga_2FeO_4) nanocrystal system was reported to exhibit LSPR around 1000 nm range.^[124] The nanocrystal shows a bipolar characteristic, that holes are majority carriers in Fe-rich samples and electrons in Ga-rich ones, and both of those can support SP. The carrier density of GFO can be tuned from $8.2 \times 10^{21} \text{ cm}^{-3}$ (Ga/Fe = 2.2, n-type) to $3.5 \times 10^{22} \text{ cm}^{-3}$ (Ga/Fe = 1.6, p-type). With high carrier density and good tenability, spinel-type oxides have important applications in photonics, especially few p-type semiconductors can excite SP in NIR.

4. Conclusion

TCOs are conventionally regarded as transparent materials in the visible range. Recently, studies have shown that TCOs have potential in infrared applications. In ENZ regime, there are strongly nonlinear effects and zero-index phenomena on TCOs. In the wavelength regime longer than ENZ, the TCOs have emerged as suitable surface plasmon materials which are alternatives to noble metals.

Carrier density plays an important role in the infrared applications of TCOs. Those with high carrier density, such as ITO and AZO, have a shorter ENZ wavelength, enabling themselves supporting surface plasmon modes in near-infrared range, especially within the communication band. By means of decreasing carrier density and increasing carrier mobility, the optical loss can be further reduced. For instance, fluorine-doped cadmium oxide reduces imaginary part of permittivity less than 1 with carrier mobility of $248 \text{ cm}^2 \text{ V}^{-1} \text{ s}^{-1}$, but the carrier density is $1.46 \times 10^{20} \text{ cm}^{-3}$, red-shifting surface plasmon regime to the mid-infrared range (around $3 \mu\text{m}$). There is no versatile material, and we need to optimize the properties of materials according to the application scenario. Fortunately, there is more improvement space for TCOs, which possess tunable optical and electric properties, low-loss, and CMOS compatibility. For example, the carrier density of doped indium oxide can be adjusted $1 \times 10^{20} \text{ cm}^{-3}$ to $6 \times 10^{21} \text{ cm}^{-3}$ by various processes. The CMOS compatibility makes TCO easy to integrate into optoelectronic devices. On the other hand, more types transparent conductive materials are discovered and studied

in recent years, such as graphene, spinel type oxides and ultrathin metals, which undoubtedly give way to the promising future for TCOs in the field of NIR wavelength.

Acknowledgements

This research was supported by the National Natural Science Foundation of China (No. 61575176), the National Basic Research Program of China (973 Program, No.2013CB632104) and the Research Foundation of State Key Laboratory of Modern Optical Instrumentation (MOI20170001).

Conflict of Interest

The authors declare no conflict of interest.

Keywords

epsilon near zero, near-infrared, surface plasmon, transparent conductive oxides

Received: October 19, 2017

Revised: January 11, 2019

Published online: February 26, 2019

- [1] H. Hosono, H. Ohta, M. Orita, K. Ueda, M. Hirano, *Vacuum* **2002**, 66, 3.
- [2] C. G. Granqvist, A. Azens, P. Heszler, L. Kish, L. Österlund, *Sol. Energy Mater. Sol. Cells* **2007**, 91, 4.
- [3] D. White, M. Feldman, *Electron. Lett.* **1970**, 6, 26.
- [4] C. G. Granqvist, *Sol. Energy Mater. Sol. Cells* **2007**, 91, 17.
- [5] K. Nomura, H. Ohta, A. Takagi, T. Kamiya, M. Hirano, H. Hosono, *Nature* **2004**, 432, 7016.
- [6] G. V. Naik, V. M. Shalae, A. Boltasseva, *Adv. Mater.* **2013**, 25, 24.
- [7] I. Liberal, N. Engheta, *Nat. Photonics* **2017**, 11, 3.
- [8] L. Caspani, R. Kaipurath, M. Clerici, M. Ferrera, T. Roger, J. Kim, N. Kinsey, M. Pietrzyk, A. Di Falco, V. M. Shalae, *Phys. Rev. Lett.* **2016**, 116, 23.
- [9] W. L. Barnes, A. Dereux, T. W. Ebbesen, *Nature* **2003**, 424, 6950.
- [10] S. A. Maier, M. L. Brongersma, P. G. Kik, S. Meltzer, A. A. Requicha, H. A. Atwater, *Adv. Mater.* **2001**, 13, 19.
- [11] S. Lal, S. Link, N. J. Halas, *Nat. Photonics* **2007**, 1, 11.
- [12] H. Hosono, D. C. Paine, *Handbook of Transparent Conductors*. Springer Science & Business Media, Berlin, Germany **2010**.
- [13] H. Kawazoe, H. Yanagi, K. Ueda, H. Hosono, *MRS Bull.* **2000**, 25, 8.
- [14] A. Kudo, H. Yanagi, H. Hosono, H. Kawazoe, *Appl. Phys. Lett.* **1998**, 73, 2.
- [15] K. H. Zhang, K. Xi, M. G. Blamire, R. G. Egdell, *J. Phys.: Condens. Matter* **2016**, 28, 38.
- [16] H. Hosono, *Thin Solid Films* **2007**, 515, 15.
- [17] X. Fang, C. Mak, S. Zhang, Z. Wang, W. Yuan, H. Ye, *J. Phys.: Condens. Matter* **2016**, 28, 22.
- [18] K. Ellmer, *Nat. Photonics* **2012**, 6, 12.
- [19] A. Boltasseva, V. M. Shalae, *Science* **2015**, 347, 6228.
- [20] F. U. Hamelmann, *J. Phys.: Conf. Ser.* Thin film zinc oxide deposited by CVD and PVD. Velingrad, Bulgaria, Hawaii **2016**, 7.
- [21] Y. Suda, H. Kawasaki, T. Ohshima, Y. Yagyu, T. Ihara, M. Yamauchi, APS Gaseous Electronics Conf., Preparation of mixed metal thin

- films by a PVD method using several kinds of powder targets. Honolulu, 10, **2015**.
- [22] C. Chen, Z. Wang, K. Wu, H. Chong, Z. Xu, H. Ye, *ACS Appl. Mater. Interfaces* **2018**, 10, 17.
- [23] G. V. Naik, J. Kim, A. Boltasseva, *Opt. Mater. Express* **2011**, 1, 6.
- [24] D. Traviss, R. Bruck, B. Mills, M. Abb, O. L. Muskens, *Appl. Phys. Lett.* **2013**, 102, 12.
- [25] M. Z. Alam, I. De Leon, R. W. Boyd, *Science* **2016**, aae0330.
- [26] H. Han, L. Cai, B. Xiang, Y. Jiang, H. Hu, *Opt. Mater. Express* **2015**, 5, 11.
- [27] C. F. Klingshirn, *Semiconductor Optics*. Springer Science & Business Media, Berlin, Germany **2012**.
- [28] H. Fujiwara, *Spectroscopic Ellipsometry: Principles and Applications*. Wiley, Hoboken, NJ, USA **2007**.
- [29] E. Hecht, *Optics*. Addison-Wesley, San Francisco, US **2002**.
- [30] N. Engheta, *Science* **2013**, 340, 6130.
- [31] S. Mário, E. Nader, *Phys. Rev. Lett.* **2006**, 97, 15.
- [32] C. Clavero, *Nat. Photonics* **2014**, 8, 2.
- [33] P. K. Jain, X. Huang, I. H. El-Sayed, M. A. El-Sayed, *Plasmonics*, **2007**, 2, 3.
- [34] W. A. Murray, W. L. Barnes, *Adv. Mater.* **2007**, 19, 22.
- [35] S. A. Maier, H. A. Atwater, *J. Appl. Phys.* **2005**, 98, 1.
- [36] L. Dai, L. Song, Y. Huang, L. Zhang, X. Lu, J. Zhang, T. Chen, *Langmuir* **2017**, 33, 22.
- [37] P. R. West, S. Ishii, G. V. Naik, N. K. Emani, V. M. Shalae, A. Boltasseva, *Laser Photonics Rev.* **2010**, 4, 6.
- [38] G. Haacke, *J. Appl. Phys.* **1976**, 47, 9.
- [39] W. T. Hsieh, P. C. Wu, J. B. Khurgin, D. P. Tsai, N. Liu, G. Sun, *ACS Photonics* **2017**, 5, 7.
- [40] J. Gwamuri, A. Vora, R. R. Khanal, A. B. Phillips, M. J. Heben, D. O. Guney, P. Bergstrom, A. Kulkarni, J. M. Pearce, *Mater. Renew. Sustain. Energy* **2015**, 4, 3.
- [41] H. G. Jerrard, *Opt. Laser Technol.* **1986**, 18, 2.
- [42] J. Frigerio, A. Ballabio, G. Isella, E. Sakat, G. Pellegrini, P. Biagioni, M. Bollani, E. Napolitani, C. Manganelli, M. Virgilio, *Phys. Rev. B* **2016**, 94, 8.
- [43] L. Zhang, Y. Zhou, L. Guo, W. Zhao, A. Barnes, H.-T. Zhang, C. Eaton, Y. Zheng, M. Brahlek, H. F. Haneef, *Nat. Mater.* **2016**, 15, 2.
- [44] Y. Zhu, R. J. Mendelsberg, J. Zhu, J. Han, A. Anders, *Appl. Surf. Sci.* **2013**, 265, 738.
- [45] C. P. Liu, Y. Foo, M. Kamruzzaman, C. Y. Ho, J. Zapien, W. Zhu, Y. Li, W. Walukiewicz, K. M. Yu, *Phys. Rev. Appl.* **2016**, 6, 6.
- [46] S. Rajak, M. Ray, *J. Opt.* **2014**, 43, 3.
- [47] C. Chen, Z. Wang, K. Wu, H. Ye, *Sci. Technol. Adv. Mater.* **2018**, 19, 1.
- [48] H. Fujiwara, M. Kondo, *Phys. Rev. B* **2005**, 71, 7.
- [49] K. Maki, N. Komiya, A. Suzuki, *Thin Solid Films* **2003**, 445, 2.
- [50] A. Comin, L. Manna, *Chem. Soc. Rev.* **2014**, 43, 11.
- [51] T. Tohsophon, A. Dabirian, S. D. Wolf, M. Morales-Masis, C. Ballif, *APL Mater.* **2015**, 3, 11.
- [52] M. Morales-Masis, S. D. Wolf, R. Woods-Robinson, J. W. Ager, C. Ballif, *Adv. Electron. Mater.* **2017**, 3, 5.
- [53] T. Koida, H. Fujiwara, M. Kondo, *Jpn. J. Appl. Phys.* **2007**, 46, 7L.
- [54] C. Guillén, J. Herrero, *J. Phys. D: Appl. Phys.* **2013**, 46, 29.
- [55] P. Guo, R. P. Chang, R. D. Schaller, *ACS Photonics* **2017**, 4, 6.
- [56] P. Guo, R. D. Schaller, L. E. Ocola, B. T. Diroll, J. B. Ketterson, R. P. Chang, *Nat. Commun.* **2016**, 7.
- [57] S. Q. Li, P. Guo, L. Zhang, W. Zhou, T. W. Odom, T. Seideman, J. B. Ketterson, R. P. Chang, *ACS Nano* **2011**, 5, 11.
- [58] M. Kang, M. Losego, E. Sachet, J.-P. Maria, S. Franzen, *ACS Photonics* **2016**, 3, 10.
- [59] C. Ye, S. Khan, Z. R. Li, E. Simsek, V. J. Sorger, *IEEE J. Sel. Top. Quantum Electron.* **2014**, 20, 4.
- [60] J.-S. Kim, J. T. Kim, *J. Phys. D: Appl. Phys.* **2016**, 49, 7.
- [61] P. Guo, R. D. Schaller, J. B. Ketterson, R. P. Chang, *Nat. Photonics* **2016**, 10, 4.
- [62] H. Wang, H. Zhao, H. Su, G. Hu, J. Zhang, *Appl. Phys. Express* **2016**, 9, 9.
- [63] B. T. Schwartz, R. Piestun, *Appl. Phys. Lett.* **2004**, 85, 1.
- [64] M. A. Badsha, Y. C. Jun, C. K. Hwangbo, *Opt. Commun.* **2014**, 332.
- [65] P. Guo, R. P. Chang, R. D. Schaller, *Appl. Phys. Lett.* **2017**, 111, 2.
- [66] A. Chaoumead, B.-H. Joo, D.-J. Kwak, Y.-M. Sung, *Appl. Surf. Sci.* **2013**, 275.
- [67] R. Gupta, K. Ghosh, S. Mishra, P. Kahol, *Appl. Surf. Sci.* **2007**, 253, 24.
- [68] R. Gupta, K. Ghosh, S. Mishra, P. Kahol, *Appl. Surf. Sci.* **2008**, 254, 6.
- [69] N. Yamada, M. Yamada, H. Toyama, R. Ino, X. Cao, Y. Yamaguchi, Y. Ninomiya, *Thin Solid Films* **2017**, 626.
- [70] R. Gupta, K. Ghosh, S. Mishra, P. Kahol, *Appl. Surf. Sci.* **2008**, 254, 13.
- [71] M. Morales-Masis, E. Rucavado, R. Monnard, L. Barraud, J. Holovsky, M. Despeisse, M. Boccard, C. Ballif, *IEEE J. Photovolt.* **2018**, 8, 5.
- [72] T. Koida, H. Fujiwara, M. Kondo, *J. Non-Cryst. Solids* **2008**, 354, 19.
- [73] E. Kobayashi, Y. Watabe, T. Yamamoto, Y. Yamada, *Sol. Energy Mater. Sol. Cells* **2016**, 149.
- [74] S. Li, Z. Shi, Z. Tang, X. Li, *J. Alloys Compd.* **2017**, 705.
- [75] J. Kim, G. V. Naik, N. K. Emani, U. Guler, A. Boltasseva, *IEEE J. Sel. Top. Quant.* **2013**, 19, 3.
- [76] J. Khurgin, Int. Congr. Adv. Electromagn. Mater. Microwaves Opt., 10th (METAMATERIALS), Replacing metals with alternative plasmonic substances in plasmonics and metamaterials: is it a good idea? Crete, Greece, 9, **2016**.
- [77] X. Fang, C. L. Mak, J. Dai, K. Li, H. Ye, C. W. Leung, *ACS Appl. Mater. Interfaces* **2014**, 6, 18.
- [78] J. C. Ndukaife, V. M. Shalae, A. Boltasseva, *Science* **2016**, 351, 6271.
- [79] J. Kim, G. V. Naik, A. V. Gavrilenko, K. Dondapati, V. I. Gavrilenko, S. Prokes, O. J. Glembocki, V. M. Shalae, A. Boltasseva, *Phys. Rev. X* **2013**, 3, 4.
- [80] S. C. Dixon, D. O. Scanlon, C. J. Carmalt, I. P. Parkin, *J. Mater. Chem. C* **2016**, 4, 29.
- [81] Z. Shu, E. Beckert, R. Eberhardt, A. Tünnermann, *J. Mater. Chem. C* **2017**, 5, 44.
- [82] H. Kim, C. Gilmore, J. Horwitz, A. Pique, H. Murata, G. Kushto, R. Schlaf, Z. Kafafi, D. Chrisey, *Appl. Phys. Lett.* **2000**, 76, 3.
- [83] G. V. Naik, J. Liu, A. V. Kildishev, V. M. Shalae, A. Boltasseva, *Proc. Natl. Acad. Sci.* **2012**, 109, 23.
- [84] J. Kim, S. Choudhury, C. DeVault, Y. Zhao, A. V. Kildishev, V. M. Shalae, A. Alù, A. Boltasseva, *ACS Nano* **2016**, 10, 10.
- [85] J. Kim, A. Dutta, B. Memarzadeh, A. V. Kildishev, H. Mosallaei, A. Boltasseva, *ACS Photonics* **2015**, 2, 8.
- [86] K. Baedeker, *Ann. Phys.* **1907**, 327, 4.
- [87] A. Dakhel, *Current Appl. Phys.* **2012**, 12, 1.
- [88] R. Maity, K. Chattopadhyay, *Sol. Energy Mater. Sol. Cells* **2006**, 90, 5.
- [89] S. Jin, Y. Yang, J. E. Medvedeva, J. R. Ireland, A. W. Metz, J. Ni, C. R. Kannewurf, A. J. Freeman, T. J. Marks, *J. Am. Chem. Soc.* **2004**, 126, 42.
- [90] Y. Dou, R. Egdell, T. Walker, D. Law, G. Beamson, *Surf. Sci.* **1998**, 398, 1.
- [91] A. Dakhel, *Phys. Status Solidi A* **2008**, 205, 11.
- [92] A. Dakhel, *Thin Solid Films* **2010**, 518, 6.
- [93] M. Yan, M. Lane, C. Kannewurf, R. Chang, *Appl. Phys. Lett.* **2001**, 78, 16.
- [94] E. Sachet, C. T. Shelton, J. S. Harris, B. E. Gaddy, D. L. Irving, S. Curtarolo, B. F. Donovan, P. E. Hopkins, P. A. Sharma, A. L. Sharma, *Nat. Mater.* **2015**, 14, 4.
- [95] P. Mazzolini, T. Acartürk, D. Chrastina, U. Starke, C. S. Casari, G. Gregori, A. L. Bassi, *Adv. Electron. Mater.* **2016**, 2, 3.

- [96] W. Wang, D. Zhang, T. Xu, X. Li, T. Zhou, X. Chen, *J. Alloys Compd.* **2002**, 335, 1.
- [97] M. A. Alim, T. Bak, A. Atanacio, J. D. Plessis, M. Zhou, J. Davis, J. Nowotny, *J. Am. Ceram. Soc.* **2017**, 100, 9.
- [98] H.-Y. Lee, J. Robertson, *J. Appl. Phys.* **2013**, 113, 21.
- [99] T. Hitosugi, Y. Furubayashi, A. Ueda, K. Itabashi, K. Inaba, Y. Hirose, G. Kinoda, Y. Yamamoto, T. Shimada, T. Hasegawa, *Jpn. J. Appl. Phys.* **2005**, 44, 8L.
- [100] P. Mazzolini, P. Gondoni, V. Russo, D. Chrastina, C. Casari, A. Li Bassi, *J. Phys. Chem. C*, **2015**, 119, 13.
- [101] T. Hitosugi, A. Ueda, S. Nakao, N. Yamada, Y. Furubayashi, Y. Hirose, T. Shimada, T. Hasegawa, *Appl. Phys. Lett.* **2007**, 90, 21.
- [102] A. Mattsson, M. Leideborg, K. Larsson, G. Westin, L. Österlund, *J. Phys. Chem. B* **2006**, 110, 3.
- [103] Y. Sato, H. Akizuki, T. Kamiyama, Y. Shigesato, *Thin Solid Films* **2008**, 516, 17.
- [104] L. Braic, N. Vasilantonakis, A. Mihai, I. J. Villar Garcia, S. Fearn, B. Zou, N. M. Alford, B. Doiron, R. F. Oulton, S. A. Maier, *ACS Appl. Mater. Interfaces* **2017**, 9, 35.
- [105] L. Dominici, F. Michelotti, T. M. Brown, A. Reale, C. A. Di, *Opt. Express* **2009**, 17, 12.
- [106] E. L. Runnerstrom, K. P. Kelley, E. Sachet, C. T. Shelton, J. P. Maria, *ACS Photonics* **2017**, 4, 8.
- [107] R. Gibson, S. Vangala, I. O. Oladeji, E. Smith, F. Khalizadeh-Rezaie, K. D. Leedy, B. Clafin, T. Cooper, R. E. Peale, J. W. Cleary, *Opt. Mater. Express* **2017**, 7, 7.
- [108] S. Mohri, Y. Hirose, S. Nakao, N. Yamada, T. Shimada, T. Hasegawa, *J. Appl. Phys.* **2012**, 111, 9.
- [109] F. Khalilzadeh-Rezaie, I. O. Oladeji, J. W. Cleary, N. Nader, J. Nath, I. Rezadad, R. E. Peale, *Opt. Mater. Express* **2015**, 5, 10.
- [110] Y. Sago, H. Fujiwara, *Jpn. J. Appl. Phys.* **2012**, 51, 10S.
- [111] X. Yang, Z. Sun, T. Low, H. Hu, X. Guo, F. J. G. D. Abajo, P. Avouris, Q. Dai, *Adv. Mater.* **2018**, 30, 20.
- [112] M. Jablan, H. Buljan, M. Soljačić, *Phys. Rev. B* **2009**, 80, 24.
- [113] M. A. Othman, C. Guclu, F. Capolino, *J. Nanophotonics* **2013**, 7, 1.
- [114] D. Rodrigo, O. Limaj, D. Janner, D. Etezadi, F. J. G. De Abajo, V. Pruneri, H. Altug, *Science* **2015**, 349, 6244.
- [115] A. Kumar, C. Zhou, *ACS Nano* **2010**, 4, 1.
- [116] J. Wu, M. Agrawal, H. A. Becerril, Z. Bao, Z. Liu, Y. Chen, P. Peumans, *ACS Nano* **2009**, 4, 1.
- [117] F. J. Garcia de Abajo, *ACS Photonics* **2014**, 1, 3.
- [118] J. Yun, *Adv. Funct. Mater.* **2017**, 27, 18.
- [119] D. N. Basov, R. D. Averitt, D. Van Der Marel, M. Dressel, K. Haule, *Rev. Mod. Phys.* **2011**, 83, 2.
- [120] B. O'Connor, C. Haughn, K.-H. An, K. P. Pipe, M. Shtein, *Appl. Phys. Lett.* **2008**, 93, 22.
- [121] M. Stewart, C.-H. Yee, J. Liu, M. Kareev, R. Smith, B. Chapler, M. Varela, P. Ryan, K. Haule, J. Chakhalian, *Phys. Rev. B* **2011**, 83, 7.
- [122] T. R. Paudel, A. Zakutayev, S. Lany, M. d'Avezac, A. Zunger, *Adv. Funct. Mater.* **2011**, 21, 23.
- [123] Y. Shi, P. F. Ndione, L. Y. Lim, D. Sokaras, T.-C. Weng, A. R. Nagaraja, A. G. Karydas, J. D. Perkins, T. O. Mason, D. S. Ginley, *Chem. Mater.* **2014**, 26, 5.
- [124] C. Urso, M. Barawi, R. Gaspari, G. Sirigu, I. Kriegel, M. Zavelani-Rossi, F. Scotognella, M. Manca, M. Prato, L. De Trizio, *J. Am. Chem. Soc.* **2017**, 139, 3.
- [125] A. Ciesielski, L. Skowronski, M. Trzcinski, T. Szoplik, *Appl. Surf. Sci.* **2017**, 421.
- [126] P. B. Johnson, R.-W. Christy, *Phys. Rev. B* **1972**, 6, 12.
- [127] J.-i. Nomoto, M. Konagai, K. Okada, T. Ito, T. Miyata, T. Minami, *Thin Solid Films* **2010**, 518, 11.